© 2015. Published by The Company of Biologists Ltd | Journal of Cell Science (2015) 128, 3695-3706 doi:10.1242/jcs.166728

COMMENTARY

ARTICLE SERIES: IMAGING

Labelling and imaging of single endogenous messenger RNA particles *in vivo*

Jan-Hendrik Spille* and Ulrich Kubitscheck‡

ABSTRACT

RNA molecules carry out widely diverse functions in numerous different physiological processes in living cells. The RNA life cycle from transcription, through the processing of nascent RNA, to the regulatory function of non-coding RNA and cytoplasmic translation of messenger RNA has been studied extensively using biochemical and molecular biology techniques. In this Commentary, we highlight how single molecule imaging and particle tracking can yield further insight into the dynamics of RNA particles in living cells. In the past few years, a variety of bright and photo-stable labelling techniques have been developed to generate sufficient contrast for imaging of single endogenous RNAs *in vivo*. New imaging modalities allow determination of not only lateral but also axial positions with high precision within the cellular context, and across a wide range of specimen from yeast and bacteria to cultured cells, and even multicellular organisms or live animals. A whole range of methods to locate and track single particles, and to analyze trajectory data are available to yield detailed information about the kinetics of all parts of the RNA life cycle. Although the concepts presented are applicable to all types of RNA, we showcase here the wealth of information gained from *in vivo* imaging of single particles by discussing studies investigating dynamics of intranuclear trafficking, nuclear pore transport and cytoplasmic transport of endogenous messenger RNA.

KEY WORDS: Single-particle tracking, RNA processing, Quantitative imaging

Introduction

All genetic information stored in DNA sequences is only accessible through RNA transcripts. Non-coding RNAs (ncRNA) can fulfil catalytic and structural as well as regulatory functions (Mattick and Makunin, 2006), whereas transcription, processing and translation of messenger RNA (mRNA) define gene expression. Here, we will discuss the principal experimental requirements to image and track single RNA particles in living cells. Although we focus on imaging of mRNA, the technical considerations apply equally to other types of RNA.

Analysis of mRNA processing has long been a focus of cell biology and biophysical research using mostly biochemical and molecular biology techniques (Daneholt, 2001; Larson et al., 2009; Pederson, 2011; Rodríguez-Navarro and Hurt, 2011; Bergalet and Lécuyer, 2014). Much less is known about intracellular RNA transport. The dynamics of mRNA processing and transport play a role in gene expression, whereas its subcellular localization, as well as regulation of its transport and translation, affect cell polarity, migration and development (reviewed by Parton et al., 2014; Buxbaum et al., 2015). Already in the nucleus, mRNAs associate with numerous auxiliary proteins to form mRNA particles (mRNPs). These mRNPs can be observed using advanced imaging techniques.

In the early 1980s, transcripts were shown to localize non-randomly in *Styela* eggs and distribute differentially during embryogenesis (Jeffery et al., 1983). Microinjection of mRNA that has been labelled *in vitro* with fluorescent nucleotides shows that different mechanisms can lead to distinct subcellular localization patterns of mRNPs, such as transport by the motor proteins kinesin, dynein and myosin (Wilkie and Davis, 2001; Zimyanin et al., 2008; reviewed in Weil et al., 2010). The first successful labelling and imaging of single mRNPs *in vivo* was achieved about 10 years ago (Fusco et al., 2003). Since then, labelling techniques, optical microscopy, tracking procedures and analysis tools have evolved dramatically (for review, see Weil et al., 2010; Eliscovich et al., 2013; Pitchiaya et al., 2014). Combinations of dedicated imaging technology and *in vivo* labelling have enabled studies of nuclear export (Grünwald and Singer, 2010; Siebrasse et al., 2012; Ma et al., 2013), and observation of the three-dimensional (3D) trajectories of single RNA particles within living eukaryotic cells (Spille et al., 2015; Smith et al., 2015).

Here, we will discuss the principal experimental requirements to track single endogenous mRNPs *in vivo* – labelling and imaging modes for achieving sufficient signal-to-noise ratio (SNR) over extended time periods, overcoming the limited axial range of light microscopy imaging and appropriate data analysis tools. Finally, we will highlight the most recent quantitative results that have been obtained by tracking single endogenous mRNPs in living cells.

Methods for fluorescence labelling of endogenous mRNA

A suitable fluorescence label is crucial for the success of single-mRNP imaging *in vivo*. In this section, we briefly discuss the most widely used labelling techniques and promising developments. The approaches can be broadly divided into the categories of – often artificially introduced – RNA motifs that bind to fluorescent probes and hybridization probes that are targeted against endogenous RNA sequences (see Fig. 1).

Fluorophore-binding RNA motifs

Genetic modifications of the RNA sequence can direct fluorescence markers to the target RNA (reviewed in Rath and Rentmeister, 2015). The widely used MS2-system is an example for this approach (Bertrand et al., 1998). Here, typically, 24 copies of a unique hairpin structure (MS2 binding site, MBS) are fused to the RNA of interest. Along with the modified RNA, a construct comprising the MS2 capsid protein (MCP) and a fluorescent protein is expressed in the cells. Dimers of MCP–fluorescent-protein bind specifically and with high affinity to MBS. A certain number of MBS repeats is

Institute of Physical and Theoretical Chemistry, Rheinische Friedrich-Wilhelms-University Bonn, Wegeler Str. 12, Bonn 53115, Germany.
*Present address: Department of Physics, Massachusetts Institute of Technology, Building 68-365, 77 Massachusetts Avenue, Cambridge, MA 02139, USA.

‡Author for correspondence (u.kubitscheck@uni-bonn.de)

Journal of Cell Science

Journal of Cell Science (2015) 128, 3695-3706 doi:10.1242/jcs.166728

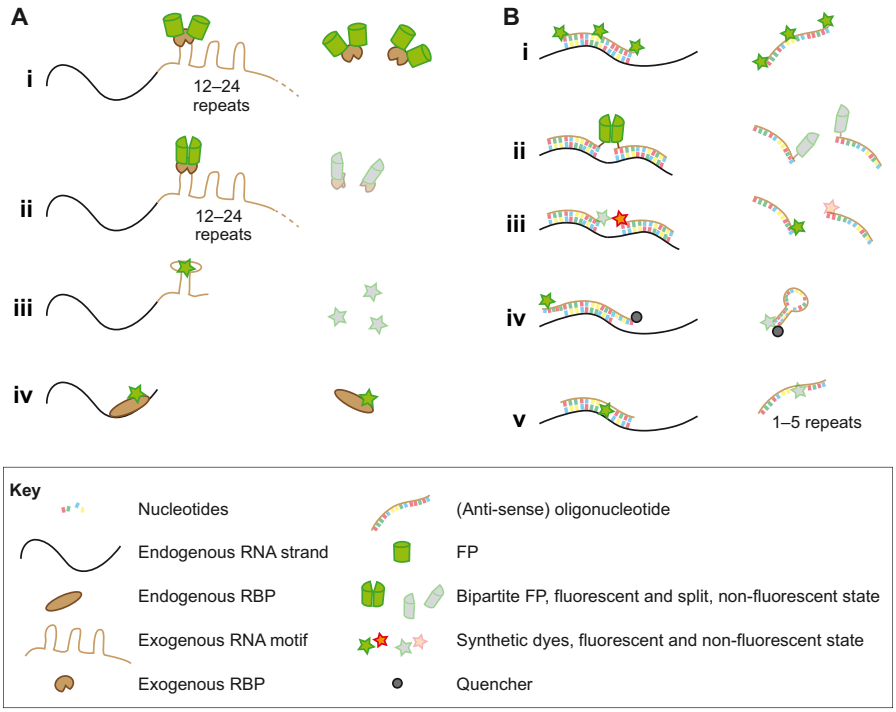

Fig. 1. Overview of RNA labelling methods. (A) RNA-binding proteins and exogenous RNA motifs. (i) Binding motifs can be introduced into the native RNA strand in order to recruit fluorescent proteins (FPs) or synthetic dye molecules to the target RNA. However, unbound fluorescent proteins, such as those used in the MS2, PP7 or λN systems, result in high unspecific background. To overcome this, fluorescent proteins can either be directed to the nucleus by coupling them with an NLS, or (ii) bipartite fluorescent proteins can be used. Similarly, an aptamer sequence can freeze the synthetic, cell-permeable dye DFHBI in a fluorescent conformation to mimic the chromophore of GFP. (iii) Endogenous expression levels can be maintained if both the modified RNA sequence and the fluorescent tag are stably incorporated into the genome. (iv) Alternatively, native RNA-binding proteins (RBPs) can be labelled *in vitro* and delivered into the cell – e.g. through microinjection. This approach enables control of the concentration of fluorescent molecules and the use of bright and stable synthetic dyes, but provides no specificity for a certain RNA species. (B) Hybridization probes. Anti-sense hybridization probes can be tailored to target an RNA sequence with high specificity, but they are not cell permeable. (i) Multiple dye molecules attached to a single probe help to increase the SNR and are particularly useful for long observations of an individual molecule. As for RNA-binding proteins, other approaches based on (ii) split fluorescent proteins, (iii and iv) energy transfer or (v) dye intercalation aim to reduce the background signal by keeping the label in a non-fluorescent state before it is bound to the RNA. Hybridization probes benefit from the use of bright and stable synthetic dyes. Care must be taken to prevent interference of the hybridization probe with the secondary structure of the target RNA and with any protein-binding motifs present.

required to raise the signal above the unspecific background level that results from unbound MCP–fluorescent-protein (Fig. 1). Traditionally, cells stably expressing the MBS sequence at the RNA of interest were transfected with MCP–fluorescent-protein, which enabled studies of intranuclear processing and transport, nuclear export and cytosolic transport of single mRNPs (reviewed in Eliscovich et al., 2013). Recently, a transgenic mouse carrying both the MBS and green fluorescent protein (GFP)-tagged MCP sequences was created, allowing the observation of β-actin mRNA at endogenous levels within live mouse tissue (Park et al., 2014).

There are similar systems that employ other proteins that bind to specific secondary RNA structures, namely the anti-terminator protein N of bacteriophage λ (λN) and the coat protein of bacteriophage PP7 (Daigle and Ellenberg, 2007; Larson et al., 2011), which enable the orthogonal labelling of multiple RNAs or of different targets on a single RNA (Lange et al., 2008; Hocine et al., 2013; reviewed in Buxbaum et al., 2015). Notably, this allows the simultaneous following of different RNA species *in vivo*, or it can be used to analyze the kinetics and precise control of mRNA splicing and translation (Martin et al., 2013; Coulon et al., 2014; Halstead et al., 2015).

The MS2 system is highly versatile and allows detection of RNA particles in many types of organisms. Recently, it has even made it possible to visualize mRNA localization in zebrafish (Campbell et al., 2015). The high background intensity that results from unbound labels is the most challenging aspect of imaging a single mRNP. Adding a nuclear localization sequence (NLS) to the labelled MCP leads to accumulation in the nucleus, whereas only mature mRNPs are exported from the nucleus. This facilitates studies of cytoplasmic mRNA trafficking by increasing the SNR. Alternatively, bipartite split fluorescent proteins have been used to render the labels non-fluorescent in their unbound state (Fig. 1) (Ozawa et al., 2007; Wu et al., 2014). Problems might arise from the length of the MBS sequence (up to 1200 nucleotides) and the size of the label, comprising up to 48 fluorescent proteins with a total molecular weight of 3 MDa (Grünwald and Singer, 2010). This could particularly be an issue if RNA dynamics are to be studied, as the diffusion constant depends on the particle size. The presence of the NLS sequence might also complicate interpretation of nuclear transport studies (Tyagi, 2009). Furthermore, labelling efficiency varies between the MCP, λN and PP7 systems, and the high number of labels might hamper quantification of RNA copy numbers.

Problems arising from overexpression of exogenous reporter systems can be circumvented by injecting proteins that have been labelled *in vitro* and bind to endogenous RNA (Siebrasse et al., 2008). This also allows for a reduction of the concentration of labelled molecules to the low levels required for single-molecule imaging.

Background suppression, similar to the split-fluorescent-protein approach, can be achieved if the protein-binding RNA sequence is replaced by an aptamer that recognizes small fluorescent ligands. For instance, the 'Spinach2' aptamer binds to the cell-permeable fluorophore 3,5-difluoro-4-hydroxybenzylidene imidazolinone (DFHBI) and increases its quantum yield upon binding (Fig. 1) (Strack et al., 2013). The fluorophore is thus only detectable if bound to the target RNA. Although it appears to be very attractive to label mRNA directly with a synthetic dye, this method has not been adopted widely, and sensitivity at the single-RNA level has not been achieved.

Other recent approaches employ molecular beacon-like quenching schemes (Sunbul and Jäschke, 2013) or Förster resonance energy transfer (FRET)-based assays (Shin et al., 2014) to suppress fluorescence of unbound probes.

Hybridization probes

Use of fluorescent proteins that bind to unique sequences in the target RNA usually requires a manipulation of the gene of interest. By contrast, probes that are fluorescently labelled *in vitro* with synthetic dyes can be targeted directly to the RNA in its endogenous or native state, as widely used in single-molecule fluorescence *in situ* hybridization (smFISH) experiments (Fig. 1B) (reviewed by Tyagi, 2009 and Armitage, 2011; Rahman and Zenklusen, 2013). In comparison to fluorescent proteins and derived fluorophores, synthetic dye molecules provide superior brightness and photostability. Both of these features are important for single-particle imaging. Because probes are synthesized and labelled *in vitro*, this approach is highly flexible with regard to the target sequence. However, the target sequence must be accessible for binding and cannot be masked by the secondary structure of the full-length RNA, or contain protein interaction sites that are essential for further processing steps. Such labelling schemes involve, for instance, oligonucleotides that carry single (Siebrasse et al., 2012) or multiple dye molecules (Spille et al., 2015), multiple adjacent probes that carry a single dye molecule each (Raj et al., 2008), or multiple probes each labelled with multiple dyes (Santangelo et al., 2009). Most often, however, this approach is used in fixed cells or tissues (Rahman and Zenklusen, 2013; Oka and Sato, 2015). For live-cell applications, the probes need to be delivered into the cells through micro-injection or membrane-permeation. This might affect the viability of the host cell, and special care must be taken to verify that cells remain viable when using any means of cell membrane perforation. Furthermore, it can also be difficult to quantify the amount of injected fluorophore.

A high background signal due to unbound probes might also arise in hybridization probes. To overcome this, approaches that combine hybridization and RNA-binding proteins have been developed. For example, targeting of the RNA sequence through hybridization was combined with the split-fluorescent-protein approach by using two probes directed against adjacent sequences in the target RNA, each carrying one part of the full fluorescent protein (Ozawa et al., 2007; Yamada et al., 2011). Similarly, side-by-side probes can be combined with a FRET pair that is split between the two probes (Cardullo et al., 1988). The presence of a quencher near the dye molecule helps to suppress the fluorescence of unbound probes. The quencher can be coupled to a second complementary oligonucleotide, which is displaced upon binding to the target sequence (Morrison et al., 1989). In so-called molecular beacons, the quencher is coupled to the same oligonucleotide (Tyagi and Kramer, 1996; Vargas et al., 2005). Molecular beacons contain small complementary sequences on both ends, thereby forcing the unbound molecule into a hairpin configuration, in which the dye and the quencher are kept in close proximity. Probe–target hybridization disrupts the hairpin structure and releases the fluorophore from the quencher to restore fluorescence emission and reveal the position of the target. More elaborate probe designs involve, for example, photoactivatable molecular beacons, which only become available for binding after irradiation with UV light, and thus allow control over the probe concentration (Rinne et al., 2013). It is essential, however, to carefully design the sequence of molecular beacons so that they function properly (Zheng et al., 2015). In view of the fact that molecular beacons were introduced about 20 years ago, their application in cell biology is still surprisingly limited. Thus, it remains unclear how useful these probes will be in enabling discoveries in the cell biology field.

In another alternative approach, oligonucleotides are not labelled through the attachment of chemical dyes but through the replacement of individual nucleotides with fluorescent surrogates (Hövelmann et al., 2014). Upon binding to the target sequence, the quantum yield is increased by intercalating the fluorophore and constraining it through a neighbouring nucleic acid that is locked in a conformation in which non-fluorescent decay pathways are effectively suppressed. This principle is similar to the aptamer approach mentioned above but does not require modifications to the endogenous RNA sequence. Owing to the low absolute brightness of the currently available intercalating fluorophores, multiple probes are required to achieve the SNR values that are required for single-RNA imaging.

Apart from the problems that arise from binding site accessibility or the blocking of protein interaction sites by the probe, RNA oligonucleotides are rapidly (within minutes) degraded within live cells. This challenge might be overcome by using 2′-O-methylribonucleotides instead of oligodeoxynucleotides (Bratu et al., 2003), or probes with stabilized backbone structures (Wu et al., 2008).

The key criteria for the successful labelling of RNA molecules for single-particle tracking are to achieve photostable and bright labelling with a sufficiently high SNR, while maintaining RNA functionality.

Optical approaches to RNA tracking – optimizing illumination and detection

The choice of the microscopy instrumentation is as important to successful imaging of single RNA particles as is the fluorescent label. The detectability of single molecules depends on the SNR as an increase in noise will make it more difficult to discern the signal from background fluctuations. Although classic epifluorescence microscopes are capable of detecting single molecules under favourable conditions, modifications to the imaging system can greatly facilitate single-RNA imaging in live cells. In the following section, we will discuss the requirements of a single-molecule-detecting microscope and the benefits of using optical sectioning methods.

Single-molecule imaging

The numerical aperture (NA) of the detection objective defines the solid angle, from which fluorescence photons emitted by the label are collected. Oil immersion can provide the highest collection efficiency at NA of approximately 1.4, but water immersion with NA in the range of 1.0 to 1.2 can be sufficient for single-molecule detection.

Fluorescence collected by the detection objective is typically cleaned up by appropriate optical filters. Narrow-band notch filters

Journal of Cell Science (2015) 128, 3695-3706 doi:10.1242/jcs.166728

can be sufficient to prevent scattered excitation light from reaching the detector, whereas band-pass filters for the fluorophore of choice can be used to suppress autofluorescence.

The signal is imaged onto a sensitive camera and yields diffraction-limited spots that are approximately half the wavelength in size. Additional magnification might be required to achieve a small image pixel size for sufficient sampling of the signal (Thompson et al., 2002). Back-illuminated electron multiplying charge-coupled device (EMCCD) cameras are most commonly used because of their low read noise and high quantum efficiency of >0.9 in the visible spectrum, but the latest generation of scientific-grade complementary metal-oxide-semiconductor (sCMOS) cameras can provide a similar sensitivity at lower cost, faster imaging speed and larger field of view (Long et al., 2012).

As mentioned above, unspecific background resulting from unbound probes is one of the biggest problems in single-RNA imaging. A number of dedicated imaging approaches have been developed to resolve this problem (see Box 1). All these methods have in common that fluorescence excitation is mostly limited to a thin layer around the focal plane of the instrument, dramatically reducing background intensity and thus increasing the SNR. An additional benefit of sectioned illumination is the reduced phototoxicity, which is particularly important for longer observation times (Reynaud et al., 2008). The optimization of image contrast by using inclined or sheet illumination is worthwhile and relatively straightforward. However, it requires a certain amount of expertise and the appropriate design of specific optical components.

Box 1. Illumination schemes for single-molecule imaging

The core building blocks (A) of a single-molecule microscope are the illumination source (Exc), typically a laser bank with multiple excitation lines covering the visible spectrum; a high numerical aperture (NA) immersion objective (Obj); a filter cube (Cub) appropriate for the dye combination; and a sensitive detector (Det), typically an EMCCD or sCMOS camera. The high NA objective limits the axial detection range to less than 1 µm. In classic epi-illumination (B), the entire cell volume is illuminated, which results in high levels of out-of-focus background fluorescence. Confocal microscopes (C) suppress background detection, but usually do not achieve sufficient sensitivity and imaging speed for single-molecule tracking owing to point-scanning of a focused laser beam (red and yellow arrows). Because out-of-focus fluorescence is still excited, photobleaching is a problem. To overcome this, sectioning can be achieved by using several dedicated illumination optics (D–G). In single-point edge-excitation sub-diffraction (SPEED) microscopy, a static point focus at an inclined angle of 45° (D) is used to observe mRNP export through single NPCs. This approach allows fast imaging rates and observation of interactions between mRNPs and a single NPC (Ma et al., 2013). Various other illumination schemes reduce background intensity by limiting fluorescence excitation to a thin sheet. The critical angle for total internal reflection can be reached by displacing the excitation beam from the centre of the objective back aperture (E). Just below the critical angle, the beam passes through the cell in a highly inclined laminated optical sheet (HILO) with a thickness of a few microns (Tokunaga et al., 2008; van't Hoff et al., 2008). This configuration yields optical sectioning up to a few microns into the specimen. In light sheet fluorescence microscopy (LSFM; F), illumination and detection optics are separated. The illumination light sheet coincides with the focal plane. Here, an excellent SNR can be obtained at depths greater than 100 µm within semi-transparent multicellular specimen (Ritter et al., 2010). For cultured cells, the light sheet can be reflected off a tip-less atomic force microscopy cantilever [reflected (r)-SPIM, Gebhardt et al., 2013; G]. The benefit of optically sectioned microscopy is a drastically increased SNR (H; adapted from Ritter et al., 2010). S, signal; N, noise; B, background.

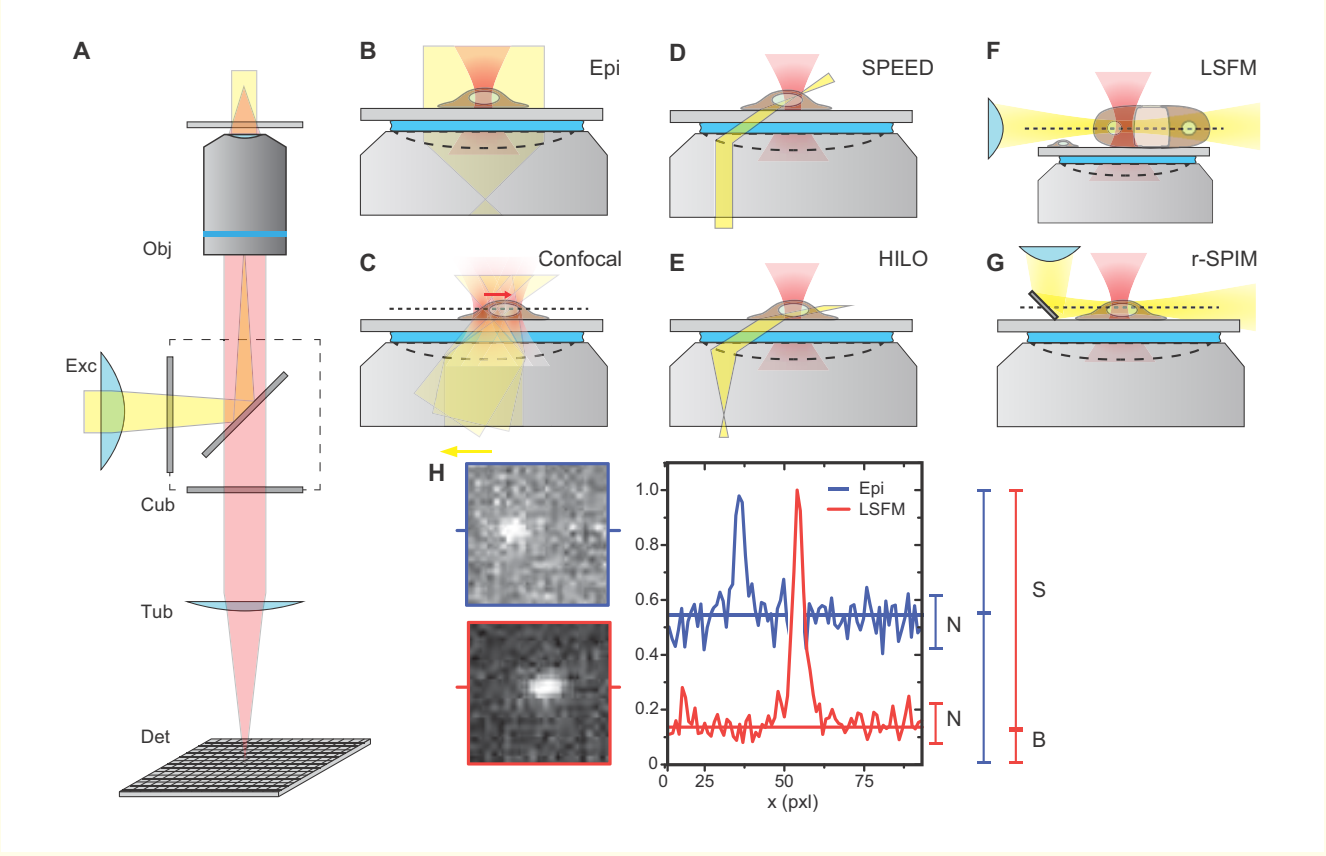

Particle detection

Owing to the high NA of the detection objective, only particles within an axial detection range of less than 1 µm around the focal plane give rise to detectable single particle signals. These will appear as intensity maxima of diffraction-limited size in the image frames as determined by the instrument point-spread function (PSF). The lateral field of view is usually orders of magnitude larger and limited by the chip size of the camera.

Typically, at least 100 photons need to be detected per frame with optical sectioning methods and several hundred photons with standard epifluorescence microscopy to achieve sufficiently bright signals. As a rule of thumb, a SNR >4 is required (Cheezum et al., 2001). Furthermore, particles should not move more than the diameter of the diffraction-limited signal during the camera exposure time to avoid blurring of the signal. Thus, frame intervals of 5–30 ms or stroboscopic illumination with light flashes of the same duration are mandatory. To resolve individual signals, the concentration of fluorescent particles must be in the picomolar range – i.e. well below one emitter per femtolitre. Even lower concentrations are required to minimize ambiguous intersections between trajectories as discussed below (see Algorithms for single-particle tracking and evaluation of tracking data).

The emitter density can be controlled by either delivering labelled probes at sufficiently low concentrations and imaging only a subset of all particles in the sample (Siebrasse et al., 2008), or by using photoactivatable probes (Manley et al., 2008; Rinne et al., 2013).

3D particle localization and feedback tracking

Without further modifications to the detection path of the microscope, particles can only be located in the two lateral dimensions. The PSF broadens symmetrically in the axial direction for particles that are not exactly located in the focal plane. Engineering the PSF to break this symmetry enables 3D localization at the nanometre scale within the axial detection range. Insertion of a cylindrical lens results in an astigmatic PSF with an elliptical shape for particles located outside the focal plane (Kao and Verkman, 1994). The major axis of the ellipsoid indicates whether the emitter is located above or below the focal plane, and its aspect ratio provides the exact deviation from the focal plane. A more elaborate phase mask can generate a PSF with the shape of a double-helix (DH-PSF) such that each emitter lights up as a doublet of intensity peaks (Pavani and Piestun, 2008). The rotation angle of the midline is a measure for the axial localization. The DH-PSF yields more isotropic localization precision and a larger axial detection range, whereas the astigmatic PSF is more photon-efficient.

Fast feedback algorithms have been employed to follow the axial path of individual particles in real-time (Juette and Bewersdorf, 2010; Spille et al., 2012). Apart from providing full spatial information, these acquisition schemes can overcome the limited detection range and substantially prolong observation periods for individual particles (Fig. 2).

The axial detection range can also be extended if multiple focal planes with axial offset are detected simultaneously on different

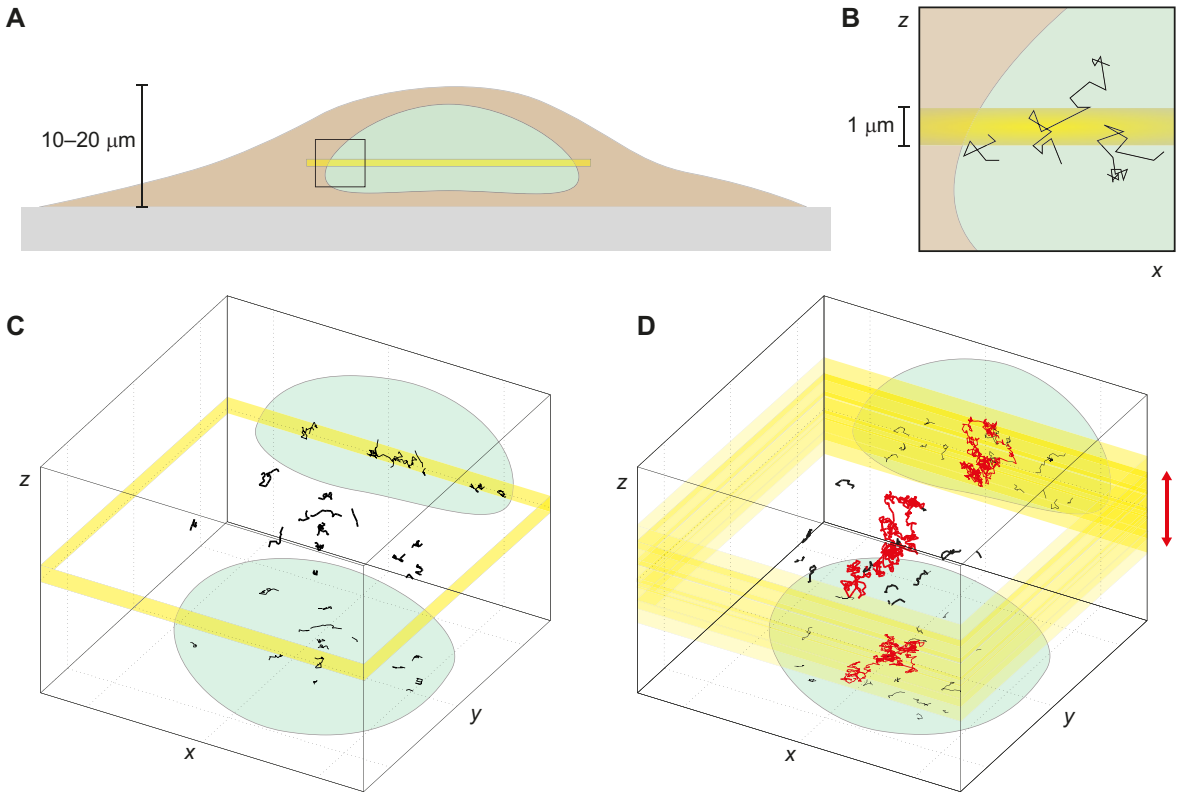

Fig. 2. 3D particle tracking over an extended axial range. (A) The detection volume in single-molecule microscopy spans a few dozen microns laterally, but typically less than 1 µm axially (yellow area). This covers the full lateral extension of a cell nucleus (green) but only a fraction of its height. (B) Diffusing particles (black lines) leave the detection volume rapidly in the axial direction and can no longer be imaged (simulated data). (C) Modifications to the detection path can be used to encode 3D coordinates with nanometric precision within the axial detection range, but obtaining trajectories remains limited to the very short times that particles are observed in this range. (D) Using feedback tracking approaches (Juette and Bewersdorf, 2010; Spille et al., 2014) or imaging systems with multiple focal planes (Smith et al., 2015) allows particles to be followed for longer time periods. The resulting trajectories (red) cover a more isotropic detection volume with extended axial range (red arrow). In addition, large numbers of short trajectories (black) are also acquired and complement the dataset.

parts of the camera chip (Ram et al., 2008). The use of up to nine planes with a separation of 250 nm can cover a substantial fraction of the nuclear volume; however, this is at the cost of a ninefold reduced intensity of signal per sub-image, not taking into account losses introduced by imperfect transmission of the required phase elements (Abrahamsson et al., 2012; Smith et al., 2015).

3D localization and long observation times can greatly enhance the information that can be deduced from RNA trajectories, as discussed in the following section (Thompson et al., 2010; Calderon et al., 2013; Spille et al., 2015; Smith et al., 2015).

Algorithms for single-particle tracking and evaluation of tracking data

To arrive at such single-particle trajectories, particles first need to be located within the images and, secondly, these locations have to be connected to trajectories. A plethora of algorithms exists for both tasks, as reviewed recently (Chenouard et al., 2014; Deschout et al., 2014; Small and Stahlheber, 2014; Sage et al., 2015). Widely used, freely available tools include u-track (Jaqaman et al., 2008) and multiple-target tracing (MTT) (Sergé et al., 2008). Both of these tools also incorporate statistical methods to resolve instances of crossing trajectories.

Most commonly, statistical properties of a trajectory ensemble are compared to a model of random diffusion owing to thermal motion. This can be achieved by analysing the distribution of particle displacements or jump distances and the mean square displacement (MSD).

The analysis of jump distance histograms gives insight into the relative fractions of particles with different mobilities, whereas the analysis of MSD plots yields two parameters, a mean diffusion coefficient D and an exponent α that indicates the type of motion (Saxton and Jacobson, 1997). Such an analysis might reveal directionality of movement, indicating active transport by motor proteins, or saltatory movement in terms of mobile and retardation phases, which indicate transient interactions (Hamilton et al., 2010; Siebrasse et al., 2008, 2012; Amrute-Nayak and Bullock, 2012). A high number of particle displacements is required to yield reliable results. Therefore, many trajectories of identical particles are pooled in a dataset and, except for the limited information contained in an MSD plot, the temporal sequence of particle displacements is disregarded. Elaborate models and long trajectories obtained by tracking particles over an extended axial range allow time to be taken into account, leading to more accurate descriptions of particle motion (Box 2).

RNA tracking in live cells

In the past few years, a number of studies have applied these experimental approaches to elucidate the pathways of RNA particles from transcription in the nucleus to translation at the cytoplasmic ribosomes.

Intranuclear mRNA trafficking

The mobility of the transcribed RNA in the cell nucleus has been examined since the 1990s (reviewed in Pederson, 2011). In a landmark paper, Politz et al. examined the mobility of mRNAs that they had labelled with fluorescent poly(T)-DNA-oligonucleotides by using fluorescence correlation spectroscopy (FCS) (Politz et al., 1998). Depending on the exact positioning of their focal detection volume of about $0.3\times0.3\times1\ \mu m^3$ within the nucleus, they measured diffusion coefficients of up to $9\ \mu m^2/s$ (Politz et al., 1998, 1999). By contrast, subsequent measurements using fluorescence recovery after photobleaching (FRAP) of RNA-poly(A)-binding protein II complexes (Calapez et al., 2002) and fluorescence activation of mRNAs labelled with poly(T)-DNA-oligonucleotides conjugated to caged fluorescein (Politz et al., 1999) yielded diffusion coefficients that were more than tenfold lower ($0.6\ \mu m^2/s$). The authors speculated that this discrepancy was caused by the inhomogeneity of the molecular intranuclear surroundings (Politz et al., 1999); chromatin is organized into chromosome territories (Pederson, 2011), and the mobility of mRNPs is generally confined to the space between these territories, the so-called interchromatin compartment. The interchromatin compartment represents a transient 3D network of small channels and larger caverns, especially near NPCs. The motion of mRNPs in such a network has been simulated, suggesting that dense chromatin layers lead to rapid transport by reducing the effective volume for diffusion, but that they can also significantly slow down intranuclear transport because of the low mobility of mRNPs that accidentally become trapped in the dense layer (Roussel and Tang, 2012). In addition, the nucleus is a complex structure of numerous nuclear organelles, which also affect the mobility of mRNPs (Grünwald et al., 2008). Thus, relatively unhindered diffusion of mRNPs in the interchromatin compartment occurs only over short distances and periods of time. Photobleaching and photoactivation techniques that measure the effective transport across large areas in the nucleus yield low effective diffusion coefficients, whereas FCS approaches that examine the local mobility (possibly within the interchromatin compartment) can yield high coefficients.

The preferential transport of mRNPs through the interchromatin compartment has been directly confirmed by Vargas et al. who introduced multiple engineered binding sites for molecular beacons into the sequence of a target RNA (Vargas et al., 2005). Fluorescently labelled molecular beacons were then microinjected into cells where they bound to transcribed RNA. Using sensitive dual-colour epifluorescence video microscopy to image single fluorescent mRNPs in respective nuclei that expressed histone 2B (H2B)–GFP as marker for chromatin allowed the authors to show that mRNPs indeed move preferentially along dedicated pathways that corresponded to intranuclear domains devoid of H2B (Fig. 3) – the interchromatin compartment (Vargas et al., 2005). Shortly before, Shav-Tal and colleagues had used the MS2 system to label and track single-RNA particles in order to clearly demonstrate that intranuclear RNA transport does not use the actin–myosin system but, instead, that it purely depends on thermal motion (Shav-Tal et al., 2004; Mor et al., 2010). However, in these initial single-RNA-particle tracking experiments, the measured diffusion coefficients were quite low ($0.01–0.09\ \mu m^2/s$) and likely to be the consequence of low imaging rates and a specific trajectory analysis.

Recent results using high-speed single-molecule imaging have demonstrated that RNA particles move as fast as theoretically expected for particles of corresponding size in the effective nuclear viscosity, which is in the range of 3 to 10 centipoise (Siebrasse et al., 2008; Veith et al., 2010; Grünwald and Singer, 2010; Ma et al., 2013). For example, Grünwald and Singer have determined a maximum diffusion coefficient of $1.4\ \mu m^2/s$ for an RNA the size of 3.3 kb (Grünwald and Singer, 2010), whereas Veith et al. have found values of 0.3 and $0.7\ \mu m^2/s$ for the particularly bulky Balbiani ring mRNPs (with a diameter of around 50 nm) in the nuclei of the salivary gland cells of *Chironomus tentans* (Veith et al., 2010). These diffusion coefficients confirm the initially obtained values (Politz et al., 1998). Several studies demonstrate that it is not only proteins that exhibit a complex pattern of

Journal of Cell Science (2015) 128, 3695-3706 doi:10.1242/jcs.166728

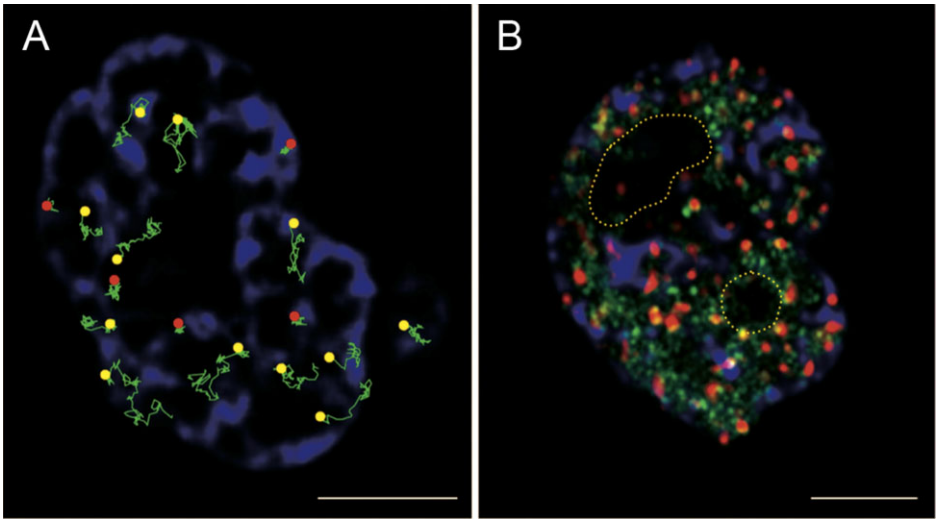

Fig. 3. mRNP motion in the cell nucleus. mRNPs move preferentially within the interchromatin compartment in cell nuclei. Chromatin-dense regions and nucleoli exclude large mRNPs. (A) Pathways of mRNPs (green) in a cell nucleus plotted onto an image of chromatin density (blue). Chromatin was labelled with H2B–GFP. Mobile particle tracks are marked by yellow dots, whereas stationary particles are marked by red dots. (B) Intranuclear regions that are frequently visited by mRNPs during the 42 s of observation time. Regions with immobile and mobile particles are marked in red and green, respectively. Chromatin is again shown in blue. The dotted lines indicate the positions of the nucleoli as seen by differential interference contrast. Scale bars: 5 µm. Images reproduced with permission from Vargas et al. (2005). Copyright (2005) National Academy of Sciences, USA.

mobility (Goulian and Simon, 2000; Kues et al., 2001; Bancaud et al., 2009), but also mRNPs that diffuse in the nucleus; their mobility cannot be described by a single diffusion coefficient (Shav-Tal et al., 2004; Siebrasse et al., 2008; Veith et al., 2010; Ma et al., 2013).

Even individual RNA particles display a discontinuous mobility, in which phases of retardation alternate with phases of higher mobility, as concluded from observations of single native mRNPS in live salivary gland cells of *C. tentans* (Siebrasse et al., 2008; Veith et al., 2010). *C. tentans is* a well-established model system that, for decades, has been used to study various aspects of the mRNA life cycle (Daneholt, 2001). Its gland cell nuclei contain four polytene chromosomes, which comprise thousands of perfectly aligned chromatids. Owing to this chromosome organization, the nuclei exhibit large areas that are devoid of chromatin, where single mRNPs can be tracked without chromatin interference. But, even in this relatively well-defined and virtually isotropic environment, a discontinuous mobility of RNA particles has been detected (Siebrasse et al., 2008; Veith et al., 2010). Only recently have we been able to characterize the duration of the various mobility phases (Spille et al., 2015). Using a light sheet microscope (Box 1) equipped with an active feedback mechanism, we observed mRNP trajectories in 3D that lasted for up to 16 s. Within these trajectories that extended over hundreds of positions, we were able to determine statistically significant phases of retarded diffusion that extended over 0.5 s (Fig. 4). It is likely that retarded motion was due to transient interactions of mRNPs with large intranuclear compounds, possibly components of the RNA processing machinery, such as splicing, export or polyadenylation factors.

Taken together, single-particle RNA tracking has revealed that intranuclear RNA transport is fast and occurs passively. Within seconds, mRNPs travel along the interchromatin compartment from the site of transcription towards the nuclear envelope, their site of nuclear export.

Nucleocytoplasmic transport

Transcription and translation in eukaryotes are spatially separated by the double membrane of the nuclear envelope. Transport across this border occurs through nuclear pore complexes (NPCs), which are embedded in the nuclear envelope. Translocation across the NPCs represents a major step of RNA trafficking and is highly regulated (reviewed in Ptak et al., 2014). The passage of RNA requires transport receptors, Mex67–Mtr2 in yeast or NXF1–NXT1 in mammalian cells, and receptor binding is an integral part of mRNP biogenesis. At the cytoplasmic face of the NPC, the export factors are actively removed from the mRNP through the action of the DEAD box helicase Dbp5 together with Gle1 and inositol hexakisphosphate (IP_6), presumably preventing the return of the

Box 2. Detecting changes in particle mobility

A number of publications have analyzed single-particle tracking data in great detail in order to detect changes in particle mobility that reflect, for example, binding states, and random, corralled or directed motion. Persson et al. introduced a complex tool for the analysis of large trajectory ensembles (vbSPT, Persson et al., 2013). Using rigorous statistical analysis, the most probable number of diffusive states is computed, and each particle localization is assigned to one of the states. Therefore, transition kinetics between mobility states can be derived. For accurate results, large datasets are required. In the current implementation, only random diffusion models are considered, but this enabled the creation of putative interaction maps and the derivation of transition rates between binding states from tens of thousands of short trajectories of the protein Hfq, which mediates mRNA–small-RNA (sRNA) interactions in *Escherichia coli* (Persson et al., 2013). Similarly, it has been shown that ribosomal subunits that are bound to mRNA are excluded from the nucleoid in the centre of the cell, whereas unbound subunits can access the entire *E. coli* volume (Sanamrad et al., 2014).

By contrast, imaging modalities with an extended axial detection range can be used to yield individual trajectories that comprise hundreds of localizations (Thompson et al., 2010; Spille et al., 2014). A close look at the temporal sequence of particle displacements enables the pinpointing of phases of distinct mobility states without making *a priori* assumptions about mobility models or the nature of the states. These phases are reflected by non-stochastic fluctuations in the length of particle displacements and can be subjected to further analysis to derive diffusion coefficients or transition frequencies between states, as has been demonstrated for Balbiani ring 2.1 mRNA and rRNA particles in *C. tentans* salivary gland cell nuclei (Fig. 4) (Spille et al., 2014).

Calderon et al. have presented a biophysical approach to derive the forces that act on *ARG3* mRNPs in budding yeast cells (Calderon et al., 2013). In their model, molecular interactions lead to constraint forces that keep the particle in a confined area, whereas active transport is reflected by directed forces. Segments of long trajectories can be analyzed to detect transitions between modes of particle motion (Calderon et al., 2013). Numerous other ways to analyze trajectory data are incorporated into the online tool ParticleStats (Hamilton et al., 2010). Recent additions to the multitude of available tools use Bayesian methods to infer transient transport dynamics or spatial maps of parameters (Monnier et al., 2015; El Beheiry et al., 2015).

Journal of Cell Science (2015) 128, 3695-3706 doi:10.1242/jcs.166728

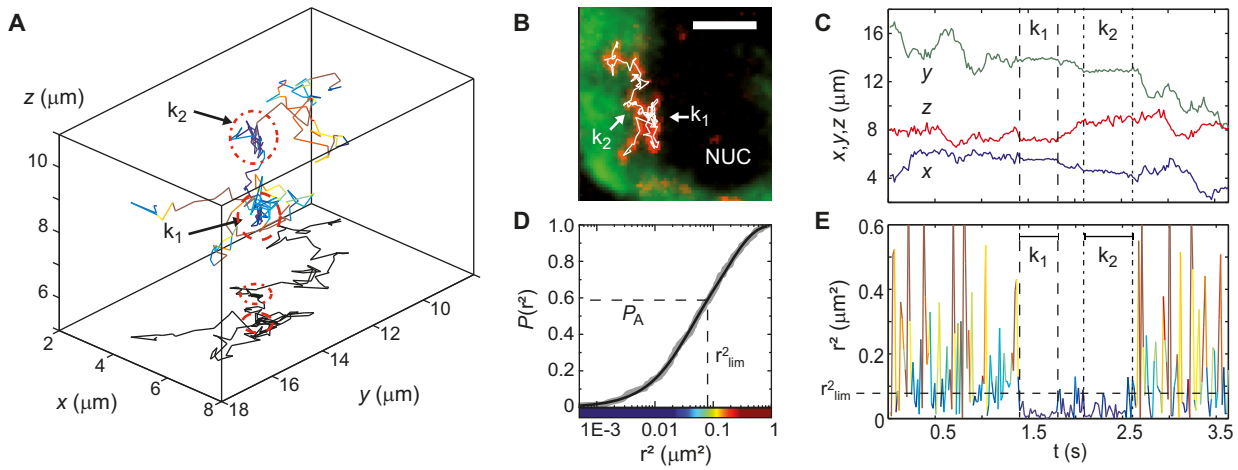

Fig. 4. Analysis of long 3D RNA particle trajectories. (A) A ribosomal (r)RNA particle was tracked inside the nucleus in feedback mode. (B) Reference images were used to put the trajectory into the structural context. Interactions with a nucleolus (NUC) led to drastically reduced mobility. (C) This plot illustrates *x*-, *y*- and *z*-coordinates of the particle as functions of time. The phases limited by the dashed lines indicate a low mobility. (D) The cumulative probability distribution $P(r^2)$ of squared jump distances r^2 between subsequent positions. Defining a threshold value r^2_{lim} assigns all steps along the trajectory either to a state of low mobility ($r^2<r^2_{lim}$) with probability $P_A=P(r^2_{lim})$ or of high mobility ($r^2\geq r^2_{lim}$). (E) Squared jump distances r^2 are shown as a function of time. Dwell times k_1 and k_2 at the nucleolus stand out as phases of low mobility with $r^2<r^2_{lim}$. Images reproduced with permission from Spille et al. (2014), *Nucleic Acids Research*, Oxford University Press.

mRNP into the nucleus (Tieg and Krebber, 2013). Nuclear RNA export can only be studied at the single-particle level, as shown in several recent studies (Mor et al., 2010; Grünwald and Singer, 2010; Siebrasse et al., 2012; Ma et al., 2013).

The authors of the first study introduced different gene constructs into mRNA that were based on human dystrophin cDNA, followed by a 3′ untranslated region (UTR) containing 24 MS2 sequence repeats (abbreviated as Dys-mRNPs) (Mor et al., 2010). The transcribed mRNA became coated with yellow fluorescent protein (YFP)-tagged MCP, and thus could be imaged using dual-channel epifluorescence microscopy while it passed through mCherry-labelled NPCs. The microscope was equipped with a slow scan charge-coupled device (CCD) camera, which did not allow for resolution of the dynamics of the actual translocation process. The maximum export duration for a 10 kb mRNA construct was estimated as 0.5 s (Mor et al., 2010).

The second study uses an epifluorescence microscope equipped with a fast EMCCD camera (Grünwald and Singer, 2010). In that study, the authors used an endogenous MCP-tagged β-actin mRNA of 3.3 kb in a stable cell line derived from a transgenic mouse and imaged its interaction with tdTomato-labelled NPCs with a time resolution of 20 ms. The authors estimated the total translocation time of this mRNA construct to be 180 ms. From their imaging data, they retrieved the distribution of mRNA binding sites along the NPC axis and found that their probe was preferentially located at both the nuclear and cytoplasmic face of the NPC with almost identical probability. The authors interpreted the former as the location of mRNA docking and the latter as the release site from the NPC. Furthermore, the authors quantified the ratio between attempted and successful mRNA translocations across the NPC, which suggested a success rate of about 36% (Grünwald and Singer, 2010).

By contrast, our study has addressed the translocation of native (not genetically manipulated) mRNPs through the NPC, combined with an analysis of the turnover kinetics of Dbp5 at the NPC (Siebrasse et al., 2012). In that study, we also made use of the cell nuclei of explanted salivary glands of *C. tentans* larvae (Siebrasse et al., 2008). To visualize native mRNPs during nuclear export, we labelled them by microinjecting the bacterially expressed and fluorescently labelled protein hrp36, which is known to associate with mRNA during mRNP assembly, whereas the nuclear envelope was labelled through co-injection of the nuclear transport factor 2 (NTF2) that had been covalently linked to AlexaFluor 546, which binds with high affinity to the very centre of the NPC (Kubitscheck et al., 2005). Using this approach, we obtained a temporal resolution of 20 ms (Siebrasse et al., 2012). Analysis of the mRNP trajectories using a kymograph approach yielded transit times that ranged from 60 ms up to 6 s. This wide range probably reflects the different sizes of the mRNPs in transit, with the large Balbiani ring mRNPs of up to 40 kb and a diameter of about 50 nm likely to require the longest times for translocation. Indeed, our ‘back-of-the-envelope’ calculation, which considered the total number of RNA molecules transcribed per second and the number of NPCs available for export, indicates that translocation times of up to 20 s should be expected for these particles, a value that is in good agreement with the experimental result (Siebrasse et al., 2012). Furthermore, a single rate-limiting step was observed, which we attribute to interactions of the RNA particles with the nuclear basket of the NPC. Possibly, this corresponds to the quality control steps known to occur at this location (Isken and Maquat, 2007). The overall success rate of mRNP export in this system is estimated to be approximately 25% (Siebrasse et al., 2012).

Ma et al. chose a different imaging approach, which allowed them to study the export of β-actin and firefly luciferase mRNAs, which they conjugated to approximately ten copies of mCherry–MCP, through single NPCs (Ma and Yang, 2010; Ma et al., 2013; reviewed by Schnell et al., 2014). They used a diffraction-limited ellipsoidal illumination volume, inclined with an angle of 45° with regard to the focal plane. Because NPCs in eukaryotic cells typically occur with an area density of 3 to 5 μm^{-2} (Kubitscheck et al., 1996), the illumination volume could be overlaid with single GFP-labelled NPCs in regions of the nuclear envelope that were less densely populated with NPCs. Owing to the small area of focus, a high irradiance was obtained, which yielded high photon rates from single mRNPs (Ma et al., 2013). Thus, the authors achieved fast imaging rates of typically 500 Hz and demonstrated that it is

important to observe the fast mRNP export process with appropriately short single frame integration times. The authors made a number of assumptions in order to extract 3D information out of the 2D imaging data, such as (i) mRNPs are transported along a direction that is perpendicular to the outline of the nuclear envelope, and (ii) mRNPs are translocated through a pore that has an inherent rotational symmetry, as well as (iii) the position of the main symmetry axis can be deduced from the GFP signal. Based on these assumptions, they developed a deconvolution algorithm to determine 3D distributions of mRNP-binding sites within the NPC from their 2D-imaging data (Ma et al., 2013). Obviously, it is not possible using this approach to deduce complete 3D trajectories of mRNPs travelling through NPCs as such owing to ambiguities in the determination of *z*-positions. Ma et al. measured a significantly shorter export duration of 12 ms for 3.3 kb mRNPs when compared to the previous results (Grünwald and Singer, 2010; Siebrasse et al., 2012) and observed that the particles primarily interact with the channel periphery on the nucleoplasmic side and in the central region of the NPC, without entering the central axial conduit. The latter result is in contradiction to a previous electron microscopy study of export factors, which showed that they bind at the very centre of the NPC (Fiserova et al., 2010). Finally, Ma et al. also report that about 36% of attempted export processes were successful. Therefore, taken together, these mRNP export studies establish that the majority of attempted export processes are not completed.

Cytoplasmic mRNA transport

After export from the nucleus, mRNA becomes available for translation in the cytoplasm. Since the 1980s, it has been known that cytoplasmic mRNAs show a localized and non-isotropic distribution in the cytoplasm (Weil et al., 2010). Thus, the distribution of cytoplasmic mRNA is due to both diffusion and active transport by kinesin, dynein and myosin, as already established in the 1990s through the microinjection of exogenous fluorescently labelled mRNA molecules into *Xenopus laevis* and *Drosophila* oocytes (for review, see Weil et al., 2010; Parton et al., 2014; Buxbaum et al., 2015). Using the MS2 system, this has also been shown for yeast and mammalian cells (Bertrand et al., 1998; Fusco et al., 2003; Ben-Ari et al., 2010).

In contrast to intranuclear mRNA trafficking, diffusion coefficients cannot accurately describe cytoplasmic mRNA transport. Particles transiently switch between active transport and diffusive motion, which requires more elaborate analysis tools that have only recently become available (see Box 2).

The localization of mRNA results in spatially inhomogeneous translation that is essential for cell and tissue development. mRNPs diffusing in the cytoplasm are more mobile than they are in the nucleus. For instance, for Dys-mRNPs, a twofold faster diffusion in the cytoplasm compared to that in the nucleus has been determined (Mor et al., 2010). However, a large fraction of the cytoplasmic mRNPs has been found to be immobile or to exhibit restricted (corralled) motion (Mor et al., 2010). In this section, we will discuss a number of recent studies on cytoplasmic mRNA transport that use advanced single-molecule imaging and analysis approaches.

The best-studied RNA is probably the β-actin mRNA (Eliscovich et al., 2013). It can be targeted to specific subcellular compartments by a zipcode protein and undergo directed transport to reach its destination (Lifland et al., 2011). β-actin mRNA is locally translated at focal adhesions, which affects the motility of cells. Notably, researchers from the Singer group have recently generated a transgenic mouse, in which all β-actin mRNA molecules carry 24 copies of the MBS motif and which co-express MCP–2×GFP (Park et al., 2014). Thus, the complete pool of endogenous β-actin mRNA is fluorescently labelled throughout the entire animal, and its localization and mobility can be probed in primary cells or even in tissue explants without any further interference. Interestingly, differences in mobility patterns between exogenous and endogenous mRNPs were observed. The authors note that a significantly smaller fraction of β-actin mRNPs exhibit directed motion in primary mouse cells. Also, the localization of mRNA was lost in immortalized, cultured cells from the transgenic mouse as compared to cells in intact tissue (Park et al., 2014). This emphasizes the fact that some aspects of mRNA trafficking might be lost in cell culture models and can only be captured in the context of complex multicellular specimens.

Another recent study from the same group reveals that β-actin mRNA, as well as ribosomal RNA, are packed into dense complexes within neuronal dendrites (Buxbaum et al., 2014). The mRNA only becomes available for translation when these granules are disassembled; this occurs upon synaptic stimulation and so provides a means of locally controlling protein concentration.

The clever use of the orthogonal labelling strategies makes completely new functional studies possible. For instance, using bacteriophage PP7 and MS2 stem–loops, a RNA biosensor has been recently developed to discriminate translated from untranslated mRNA, and to indicate the location and time point of the first round of translation (Halstead et al., 2015). In that work, PP7 stem–loops were introduced into the coding sequence, whereas MS2 stem–loops were introduced into the 3′untranslated (UTR) region, allowing these two sequence domains to be labelled by spectrally distinct fluorescent proteins; expression of GFP- and NLS-conjugated PP7 coat protein (GFP–PCP) and of red fluorescent protein (RFP)- and NLS-conjugated MCP resulted in nuclear mRNA with a green and a red label. In the cytoplasm, the first passage of the coding sequence through the ribosome removes GFP–PCP from the transcript, revealing the location and time point of the first round of translation.

Conclusions and outlook

In the past ten years, *in vivo* RNA labelling strategies and microscopy approaches to optimize single-RNA imaging with regard to improving contrast, tracking ability and image analysis have advanced dramatically. The acquisition of RNA trajectories comprising thousands of single positions is possible today, even in living tissues or live animals. In particular, new illumination and detection schemes allow the observation of RNA transport with an unprecedented spatial precision and temporal resolution. The new approaches to observe single mRNA molecules within live tissues and complete animals hold particular promise, as only such complex systems display the full range of RNA processing. The data presented so far reveal extremely complex RNA dynamics, which are far from being isotropic. It can be expected that the techniques discussed here will soon be applied to the plethora of different RNA species (for example, Fei et al., 2015), whose function in many cases is still entirely unclear. The simultaneous use of orthogonal labelling strategies and the placement of the labels into specific regions of the RNA sequence make it possible to analyze key steps of RNA processing, such as splicing and the initiation of translation (Martin et al., 2013; Halstead et al., 2015).

It remains a major challenge to precisely locate RNA particles within their 3D structural context using advanced and sufficiently

fast 3D imaging approaches. Co-labelling of interaction partners, imaging of reference frameworks and use of registration procedures in order to fully elucidate RNA particle function and regulation all present useful steps in this direction (Spille et al., 2015; Smith et al., 2015). Still, the currently available fluorescent labels limit localization precision and data acquisition speed. Further improvements in signal strength and background reduction are most desirable, and require progress in technologies for the labelling of biomolecules with fluorescent proteins or small protein tags, such as SNAP tags, for use in combination with bright cell-permeable dyes (Lukinavičius et al., 2013; Grimm et al., 2015). Ultimately, improvements in labelling and imaging technologies might make it possible to follow endogenous RNAs throughout their entire life cycle in live animals and, using elaborate analysis software, to scrutinize the kinetics of the molecular interactions in order to fully understand the mechanisms underlying RNA processing, the implications of pre-translational processing steps for gene expression and to even elucidate the functional roles of ncRNA.

Acknowledgements
The authors acknowledge Dr. J. P. Siebrasse for critical reading of the manuscript.

Competing interests
The authors declare no competing or financial interests.

Funding
Funding was provided by the German Research Foundation [grant number KU 2474/8-1]. J.-H.S. was supported by a fellowship from the German National Academic Foundation.

References
Abrahamsson, S., Chen, J., Hajj, B., Stallinga, S., Katsov, A. Y., Wisniewski, J., Mizuguchi, G., Soule, P., Mueller, F., Darzacq, C. D. et al. (2012). Fast multicolor 3D imaging using aberration-corrected multifocus microscopy. *Nat. Methods* **10**, 60-63.

Amrute-Nayak, M. and Bullock, S. L. (2012). Single-molecule assays reveal that RNA localization signals regulate dynein–dynactin copy number on individual transcript cargoes. *Nat. Cell Biol.* **14**, 416-423.

Armitage, B. A. (2011). Imaging of RNA in live cells. *Curr. Opin. Chem. Biol.* **15**, 806-812.

Bancaud, A., Huet, S., Daigle, N., Mozziconacci, J., Beaudouin, J. and Ellenberg, J. (2009). Molecular crowding affects diffusion and binding of nuclear proteins in heterochromatin and reveals the fractal organization of chromatin. *EMBO J.* **28**, 3785-3798.

Ben-Ari, Y., Brody, Y., Kinor, N., Mor, A., Tsukamoto, T., Spector, D. L., Singer, R. H. and Shav-Tal, Y. (2010). The life of an mRNA in space and time. *J. Cell Sci.* **123**, 1761-1774.

Bergalet, J. and Lécuyer, E. (2014). The functions and regulatory principles of mRNA intracellular trafficking. In *Systems Biology of RNA Binding Proteins* (ed. E. Yeo), pp. 57-96.

Bertrand, E., Chartrand, P., Schaefer, M., Shenoy, S. M., Singer, R. H. and Long, R. M. (1998). Localization of ash1 mRNA particles in living yeast. *Mol. Cell* **2**, 437-445.

Bratu, D. P., Cha, B.-J., Mhlanga, M. M., Kramer, F. R. and Tyagi, S. (2003). Visualizing the distribution and transport of mRNAs in living cells. *Proc. Natl. Acad. Sci. USA* **100**, 13308-13313.

Buxbaum, A. R., Wu, B. and Singer, R. H. (2014). Single β-actin mRNA detection in neurons reveals a mechanism for regulating its translatability. *Science* **343**, 419-422.

Buxbaum, A. R., Haimovich, G. and Singer, R. H. (2015). In the right place at the right time: visualizing and understanding mRNA localization. *Nat. Rev. Mol. Cell Biol.* **16**, 95-109.

Calapez, A., Pereira, H. M., Calado, A., Braga, J., Rino, J., Carvalho, C., Tavanez, J. P., Wahle, E., Rosa, A. C. and Carmo-Fonseca, M. (2002). The intranuclear mobility of messenger RNA binding proteins is ATP dependent and temperature sensitive. *J. Cell Biol.* **159**, 795-805.

Calderon, C. P., Thompson, M. A., Casolari, J. M., Paffenroth, R. C. and Moerner, W. E. (2013). Quantifying transient 3d dynamical phenomena of single mRNA particles in live yeast cell measurements. *J. Phys. Chem. B* **117**, 15701-15713.

Campbell, P. D., Chao, J. A., Singer, R. H. and Marlow, F. L. (2015). Dynamic visualization of transcription and RNA subcellular localization in zebrafish. *Development* **142**, 1368-1374.

Cardullo, R. A., Agrawal, S., Flores, C., Zamecnik, P. C. and Wolf, D. E. (1988). Detection of nucleic acid hybridization by nonradiative fluorescence resonance energy transfer. *Proc. Natl. Acad. Sci. USA* **85**, 8790-8794.

Cheezum, M. K., Walker, W. F. and Guilford, W. H. (2001). Quantitative comparison of algorithms for tracking single fluorescent particles. *Biophys. J.* **81**, 2378-2388.

Chenouard, N., Smal, I., de Chaumont, F., Maška, M., Sbalzarini, I. F., Gong, Y., Cardinale, J., Carthel, C., Coraluppi, S., Winter, M. et al. (2014). Objective comparison of particle tracking methods. *Nat. Methods* **11**, 281-289.

Coulon, A., Ferguson, M. L., de Turris, V., Palangat, M., Chow, C. C. and Larson, D. R. (2014). Kinetic competition during the transcription cycle results in stochastic RNA processing. *Elife* **3**, e03939.

Daigle, N. and Ellenberg, J. (2007). λN-GFP: an RNA reporter system for live-cell imaging. *Nat. Methods* **4**, 633-636.

Daneholt, B. (2001). Assembly and transport of a premessenger RNP particle. *Proc. Natl. Acad. Sci. USA* **98**, 7012-7017.

Deschout, H., Zanacchi, F. C., Mlodzianoski, M., Diaspro, A., Bewersdorf, J., Hess, S. T. and Braeckmans, K. (2014). Precisely and accurately localizing single emitters in fluorescence microscopy. *Nat. Methods* **11**, 253-266.

El Beheiry, M., Dahan, M. and Masson, J.-B. (2015). InferenceMAP: mapping of single-molecule dynamics with Bayesian inference. *Nat. Methods* **12**, 594-595.

Eliscovich, C., Buxbaum, A. R., Katz, Z. B. and Singer, R. H. (2013). mRNA on the move: the road to its biological destiny. *J. Biol. Chem.* **288**, 20361-20368.

Fei, J., Singh, D., Zhang, Q., Park, S., Balasubramanian, D., Golding, I., Vanderpool, C. K. and Ha, T. (2015). Determination of in vivo target search kinetics of regulatory noncoding RNA. *Science* **347**, 1371-1374.

Fiserova, J., Richards, S. A., Wente, S. R. and Goldberg, M. W. (2010). Facilitated transport and diffusion take distinct spatial routes through the nuclear pore complex. *J. Cell Sci.* **123**, 2773-2780.

Fusco, D., Accornero, N., Lavoie, B., Shenoy, S. M., Blanchard, J.-M., Singer, R. H. and Bertrand, E. (2003). Single mRNA molecules demonstrate probabilistic movement in living mammalian cells. *Curr. Biol.* **13**, 161-167.

Gebhardt, J. C. M., Suter, D. M., Roy, R., Zhao, Z. W., Chapman, A. R., Basu, S., Maniatis, T. and Xie, X. S. (2013). Single-molecule imaging of transcription factor binding to DNA in live mammalian cells. *Nat. Methods* **10**, 421-426.

Goulian, M. and Simon, S. M. (2000). Tracking single proteins within cells. *Biophys. J.* **79**, 2188-2198.

Grimm, J. B., English, B. P., Chen, J., Slaughter, J. P., Zhang, Z., Revyakin, A., Patel, R., Macklin, J. J., Normanno, D., Singer, R. H. et al. (2015). A general method to improve fluorophores for live-cell and single-molecule microscopy. *Nat. Methods* **12**, 244-250.

Grünwald, D. and Singer, R. H. (2010). In vivo imaging of labelled endogenous β-actin mRNA during nucleocytoplasmic transport. *Nature* **467**, 604-607.

Grünwald, D., Martin, R. M., Buschmann, V., Bazett-Jones, D. P., Leonhardt, H., Kubitscheck, U. and Cardoso, M. C. (2008). Probing intranuclear environments at the single-molecule level. *Biophys. J.* **94**, 2847-2858.

Halstead, J. M., Lionnet, T., Wilbertz, J. H., Wippich, F., Ephrussi, A., Singer, R. H. and Chao, J. A. (2015). An RNA biosensor for imaging the first round of translation from single cells to living animals. *Science* **347**, 1367-1671.

Hamilton, R. S., Parton, R. M., Oliveira, R. A., Vendra, G., Ball, G., Nasmyth, K. and Davis, I. (2010). ParticleStats: open source software for the analysis of particle motility and cytoskeletal polarity. *Nucleic Acids Res.* **38**, W641-W646.

Hocine, S., Raymond, P., Zenklusen, D., Chao, J. A. and Singer, R. H. (2013). Single-molecule analysis of gene expression using two-color RNA labeling in live yeast. *Nat. Methods* **10**, 119-121.

Hövelmann, F., Gaspar, I., Loibl, S., Ermilov, E. A., Röder, B., Wengel, J., Ephrussi, A. and Seitz, O. (2014). Brightness through local constraint-LNA-enhanced fit hybridization probes for in vivo ribonucleotide particle tracking. *Angew. Chem. Int. Ed.* **53**, 11370-11375.

Isken, O. and Maquat, L. E. (2007). Quality control of eukaryotic mRNA: safeguarding cells from abnormal mRNA function. *Genes Dev.* **21**, 1833-3856.

Jaqaman, K., Loerke, D., Mettlen, M., Kuwata, H., Grinstein, S., Schmid, S. L. and Danuser, G. (2008). Robust single-particle tracking in live-cell time-lapse sequences. *Nat. Methods* **5**, 695-702.

Jeffery, W. R., Tomlinson, C. R. and Brodeur, R. D. (1983). Localization of actin messenger RNA during early ascidian development. *Dev. Biol.* **99**, 408-417.

Juette, M. F. and Bewersdorf, J. (2010). Three-dimensional tracking of single fluorescent particles with submillisecond temporal resolution. *Nano Lett.* **10**, 4657-4663.

Kao, H. P. and Verkman, A. S. (1994). Tracking of single fluorescent particles in three dimensions: use of cylindrical optics to encode particle position. *Biophys. J.* **67**, 1291-1300.

Kubitscheck, U., Wedekind, P., Zeidler, O., Grote, M. and Peters, R. (1996). Single nuclear pores visualized by confocal microscopy and image processing. *Biophys. J.* **70**, 2067-2077.

Kubitscheck, U., Grünwald, D., Hoekstra, A., Rohleder, D., Kues, T., Siebrasse, J. P. and Peters, R. (2005). Nuclear transport of single molecules: dwell times at the nuclear pore complex. *J. Cell Biol.* **168**, 233-243.

Kues, T., Peters, R. and Kubitscheck, U. (2001). Visualization and tracking of single protein molecules in the cell nucleus. *Biophys. J.* **80**, 2954-2967.

Lange, S., Katayama, Y., Schmid, M., Burkacky, O., Bruchle, C., Lamb, D. C. and Jansen, R.-P. (2008). Simultaneous transport of different localized mRNA species revealed by live-cell imaging. *Traffic* **9**, 1256-1267.
Larson, D. R., Singer, R. H. and Zenklusen, D. (2009). A single molecule view of gene expression. *Trends Cell Biol.* **19**, 630-637.
Larson, D. R., Zenklusen, D., Wu, B., Chao, J. A. and Singer, R. H. (2011). Real-time observation of transcription initiation and elongation on an endogenous yeast gene. *Science* **332**, 475-478.
Lifland, A. W., Zurla, C., Yu, J. and Santangelo, P. J. (2011). Dynamics of native β-actin mRNA transport in the cytoplasm. *Traffic* **12**, 1000-1011.
Long, F., Zeng, S. and Huang, Z.-L. (2012). Localization-based super-resolution microscopy with an scmos camera part ii: Experimental methodology for comparing scmos with emccd cameras. *Opt. Expr.* **20**, 17741-17759.
Lukinavičius, G., Umezawa, K., Olivier, N., Honigmann, A., Yang, G., Plass, T., Mueller, V., Reymond, L., Corrêa, I. R., Jr, Luo, Z.-G. et al. (2013). A near-infrared fluorophore for live-cell super-resolution microscopy of cellular proteins. *Nat. Chem.* **5**, 132-139.
Ma, J. and Yang, W. (2010). Three-dimensional distribution of transient interactions in the nuclear pore complex obtained from single-molecule snapshots. *Proc. Natl. Acad. Sci. USA* **107**, 7305-7310.
Ma, J., Liu, Z., Michelotti, N., Pitchiaya, S., Veerapaneni, R., Androsavich, J. R., Walter, N. G. and Yang, W. (2013). High-resolution three-dimensional mapping of mRNA export through the nuclear pore. *Nat. Commun.* **4**, 2414.
Manley, S., Gillette, J. M., Patterson, G. H., Shroff, H., Hess, H. F., Betzig, E. and Lippincott-Schwartz, J. (2008). High-density mapping of single-molecule trajectories with photoactivated localization microscopy. *Nat. Methods* **5**, 155-157.
Martin, R. M., Rino, J., Carvalho, C., Kirchhausen, T. and Carmo-Fonseca, M. (2013). Live-cell visualization of pre-mRNA splicing with single-molecule sensitivity. *Cell Rep.* **4**, 1144-1155.
Mattick, J. S. and Makunin, I. V. (2006). Non-coding RNA. *Hum. Mol. Genet.* **15**, R17-R29.
Mor, A., Suliman, S., Ben-Yishay, R., Yunger, S., Brody, Y. and Shav-Tal, Y. (2010). Dynamics of single mRNP nucleocytoplasmic transport and export through the nuclear pore in living cells. *Nat. Cell Biol.* **12**, 543-552.
Morrison, L. E., Halder, T. C. and Stols, L. M. (1989). Solution-phase detection of polynucleotides using interacting fluorescent labels and competitive hybridization. *Anal. Biochem.* **183**, 231-244.
Monnier, N., Barr, Z., Park, H. Y., Su, K.-C., Katz, Z., English, B. P., Dey, A., Pan, A., Cheeseman, I. M., Singer, R. H. et al. (2015). Inferring transient particle transport dynamics in live cells. *Nat. Methods* **12**, 838-840.
Oka, Y. and Sato, T. N. (2015). Whole-mount single molecule FISH method for zebrafish embryo. *Sci. Rep.* **5**, 8571.
Ozawa, T., Natori, Y., Sato, M. and Umezawa, Y. (2007). Imaging dynamics of endogenous mitochondrial RNA in single living cells. *Nat. Methods* **4**, 413-419.
Park, H. Y., Lim, H., Yoon, Y. J., Follenzi, A., Nwokafor, C., Lopez-Jones, M., Meng, X. and Singer, R. H. (2014). Visualization of dynamics of single endogenous mRNA labeled in live mouse. *Science* **343**, 422-424.
Parton, R. M., Davidson, A., Davis, I. and Weil, T. T. (2014). Subcellular mRNA localisation at a glance. *J. Cell Sci.* **127**, 2127-2133.
Pavani, S. R. P. and Piestun, R. (2008). Three dimensional tracking of fluorescent microparticles using a photon-limited double-helix response system. *Opt. Expr.* **16**, 22048-22057.
Pederson, T. (2011). The nucleus introduced. *Cold Spring Harb. Perspect. Biol.* **3**, a000521.
Persson, F., Lindén, M., Unoson, C. and Elf, J. (2013). Extracting intracellular diffusive states and transition rates from single-molecule tracking data. *Nat. Methods* **10**, 265-269.
Pitchiaya, S., Heinicke, L. A., Custer, T. C. and Walter, N. G. (2014). Single molecule fluorescence approaches shed light on intracellular RNAs. *Chem. Rev.* **114**, 3224-3265.
Politz, J. C., Browne, E. S., Wolf, D. E. and Pederson, T. (1998). Intranuclear diffusion and hybridization state of oligonucleotides measured by fluorescence correlation spectroscopy in living cells. *Proc. Natl. Acad. Sci. USA* **95**, 6043-6048.
Politz, J. C., Tuft, R. A., Pederson, T. and Singer, R. H. (1999). Movement of nuclear poly(A) RNA throughout the interchromatin space in living cells. *Curr. Biol.* **9**, 285-291.
Ptak, C., Aitchison, J. D. and Wozniak, R. W. (2014). The multifunctional nuclear pore complex: a platform for controlling gene expression. *Curr. Opin. Cell Biol.* **28**, 46-53.
Rahman, S. and Zenklusen, D. (2013). Single-molecule resolution fluorescent in situ hybridization (smFISH) in the yeast S. cerevisiae. *Methods Mol. Biol.* **1042**, 33-46.
Raj, A., Van Den Bogaard, P., Rifkin, S. A., van Oudenaarden, A. and Tyagi, S. (2008). Imaging individual mRNA molecules using multiple singly labeled probes. *Nat. Methods* **5**, 877-879.
Ram, S., Prabhat, P., Chao, J., Sally Ward, E. and Ober, R. J. (2008). High accuracy 3D quantum dot tracking with multifocal plane microscopy for the study of fast intracellular dynamics in live cells. *Biophys. J.* **95**, 6025-6043.
Rath, A. K. and Rentmeister, A. (2015). Genetically encoded tools for RNA imaging in living cells. *Curr. Opin. Biotech.* **31**, 42-49.
Reynaud, E. G., Kržič, U., Greger, K. and Stelzer, E. H. K. (2008). Light sheet-based fluorescence microscopy: more dimensions, more photons, and less photodamage. *HFSP J.* **2**, 266-275.
Rinne, J. S., Kaminski, T. P., Kubitscheck, U. and Heckel, A. (2013). Light-inducible molecular beacons for spatio-temporally highly defined activation. *Chem. Commun.* **49**, 5375-5377.
Ritter, J. G., Veith, R., Veenendaal, A., Siebrasse, J. P. and Kubitscheck, U. (2010). Light sheet microscopy for single molecule tracking in living tissue. *PLoS ONE* **5**, e11639.
Rodríguez-Navarro, S. and Hurt, E. (2011). Linking gene regulation to mRNA production and export. *Curr. Opin. Cell Biol.* **23**, 302-309.
Roussel, M. R. and Tang, T. (2012). Simulation of mRNA diffusion in the nuclear environment. *IET Syst. Biol.* **6**, 125-133.
Sage, D., Kirshner, H., Pengo, T., Stuurman, N., Min, J., Manley, S. and Unser, M. (2015). Quantitative evaluation of software packages for single-molecule localization microscopy. *Nat. Methods* **12**, 717-724.
Sanamrad, A., Persson, F., Lundius, E. G., Fange, D., Gynnå, A. H. and Elf, J. (2014). Single-particle tracking reveals that free ribosomal subunits are not excluded from the escherichia coli nucleoid. *Proc. Natl. Acad. Sci. USA* **111**, 11413-11418.
Santangelo, P. J., Lifland, A. W., Curt, P., Sasaki, Y., Bassell, G. J., Lindquist, M. E. and Crowe, J. E. (2009). Single molecule–sensitive probes for imaging RNA in live cells. *Nat. Methods* **6**, 347-349.
Saxton, M. J. and Jacobson, K. (1997). Single-particle tracking: applications to membrane dynamics. *Ann. Rev. Biophys. Biomol. Struct.* **26**, 373-399.
Schnell, S. J., Ma, J. and Yang, W. (2014). Three-dimensional mapping of mRNA export through the nuclear pore complex. *Genes* **5**, 1032-1049.
Sergé, A., Bertaux, N., Rigneault, H. and Marguet, D. (2008). Dynamic multiple-target tracing to probe spatiotemporal cartography of cell membranes. *Nat. Methods* **5**, 687-694.
Shav-Tal, Y., Darzacq, X., Shenoy, S. M., Fusco, D., Janicki, S. M., Spector, D. L. and Singer, R. H. (2004). Dynamics of single mRNPs in nuclei of living cells. *Science* **304**, 1797-1800.
Shin, I., Ray, J., Gupta, V., Ilgu, M., Beasley, J., Bendickson, L., Mehanovic, S., Kraus, G. A. and Nilsen-Hamilton, M. (2014). Live-cell imaging of pol II promoter activity to monitor gene expression with RNA image tag reporters. *Nucleic Acids Res.* **42**, e90.
Siebrasse, J. P., Veith, R., Dobay, A., Leonhardt, H., Daneholt, B. and Kubitscheck, U. (2008). Discontinuous movement of mRNP particles in nucleoplasmic regions devoid of chromatin. *Proc. Natl. Acad. Sci. USA* **105**, 20291-20296.
Siebrasse, J. P., Kaminski, T. and Kubitscheck, U. (2012). Nuclear export of single native mRNA molecules observed by light sheet fluorescence microscopy. *Proc. Natl. Acad. Sci. USA* **109**, 9426-9431.
Small, A. and Stahlheber, S. (2014). Fluorophore localization algorithms for super-resolution microscopy. *Nat. Methods* **11**, 267-279.
Smith, C. S., Preibisch, S., Joseph, A., Abrahamsson, S., Rieger, B., Myers, E., Singer, R. H. and Grunwald, D. (2015). Nuclear accessibility of β-actin mRNA is measured by 3D single-molecule real-time tracking. *J. Cell Biol.* **209**, 609-619.
Spille, J.-H., Kaminski, T., Königshoven, H.-P. and Kubitscheck, U. (2012). Dynamic three-dimensional tracking of single fluorescent nanoparticles deep inside living tissue. *Opt. Expr.* **20**, 19697-19707.
Spille, J.-H., Kaminski, T. P., Scherer, K., Rinne, J. S., Heckel, A. and Kubitscheck, U. (2015). Direct observation of mobility state transitions in RNA trajectories by sensitive single molecule feedback tracking. *Nucleic Acids Res.* **43**, e14.
Strack, R. L., Disney, M. D. and Jaffrey, S. R. (2013). A superfolding spinach2 reveals the dynamic nature of trinucleotide repeat–containing RNA. *Nat. Methods* **10**, 1219-1224.
Sunbul, M. and Jäschke, A. (2013). Contact-mediated quenching for RNA imaging in bacteria with a fluorophore-binding aptamer. *Angew. Chem. Int. Ed.* **52**, 13401-13404.
Thompson, R. E., Larson, D. R. and Webb, W. W. (2002). Precise nanometer localization analysis for individual fluorescent probes. *Biophys. J.* **82**, 2775-2783.
Thompson, M. A., Casolari, J. M., Badieirostami, M., Brown, P. O. and Moerner, W. E. (2010). Three-dimensional tracking of single mRNA particles in *Saccharomyces Cerevisiae* using a double-helix point spread function. *Proc. Natl. Acad. Sci. USA* **107**, 17864-17871.
Tieg, B. and Krebber, H. (2013). Dbp5—from nuclear export to translation. *Biochim. Biophys. Acta* **1829**, 791-798.
Tokunaga, M., Imamoto, N. and Sakata-Sogawa, K. (2008). Highly inclined thin illumination enables clear single-molecule imaging in cells. *Nat. Methods* **5**, 159-161.
Tyagi, S. (2009). Imaging intracellular RNA distribution and dynamics in living cells. *Nat. Methods* **6**, 331-338.
Tyagi, S. and Kramer, F. R. (1996). Molecular beacons: probes that fluoresce upon hybridization. *Nat. Biotech.* **14**, 303-308.
van't Hoff, M., de Sars, V. and Oheim, M. (2008). A programmable light engine for quantitative single molecule TIRF and HiLo imaging. *Opt. Expr.* **16**, 18495-18504.

Vargas, D. Y., Raj, A., Marras, S. A. E., Kramer, F. R. and Tyagi, S. (2005). Mechanism of mRNA transport in the nucleus. *Proc. Natl. Acad. Sci. USA* **102**, 17008-17013.
Veith, R., Sorkalla, T., Baumgart, E., Anzt, J., Häberlein, H., Tyagi, S., Siebrasse, J. P. and Kubitscheck, U. (2010). Balbiani ring mRNPs diffuse through and bind to clusters of large intranuclear molecular structures. *Biophys. J.* **99**, 2676-2685.
Weil, T. T., Parton, R. M. and Davis, I. (2010). Making the message clear: visualizing mRNA localization. *Trends Cell Biol.* **20**, 380-390.
Wilkie, G. S. and Davis, I. (2001). Drosophila wingless and pair-rule transcripts localize apically by dynein-mediated transport of RNA particles. *Cell* **105**, 209-219.
Wu, Y., Yang, C. J., Moroz, L. L. and Tan, W. (2008). Nucleic acid beacons for long-term real-time intracellular monitoring. *Anal. Chem.* **80**, 3025-3028.
Wu, B., Chen, J. and Singer, R. H. (2014). Background free imaging of single mRNAs in live cells using split fluorescent proteins. *Sci. Rep.* **4**, 3615.
Yamada, T., Yoshimura, H., Inaguma, A. and Ozawa, T. (2011). Visualization of nonengineered single mRNAs in living cells using genetically encoded fluorescent probes. *Anal. Chem.* **83**, 5708-5714.
Zheng, J., Yang, R., Shi, M., Wu, C., Fang, X., Li, Y., Li, J. and Tan, W. (2015). Rationally designed molecular beacons for bioanalytical and biomedical applications. *Chem. Soc. Rev.* **44**, 3036-3055.
Zimyanin, V. L., Belaya, K., Pecreaux, J., Gilchrist, M. J., Clark, A., Davis, I. and St Johnston, D. (2008). In vivo imaging of oskar mRNA transport reveals the mechanism of posterior localization. *Cell* **134**, 843-853.